Antarctic Science 15 (2): 271–282 (2003) © Antarctic Science Ltd Printed in the UK DOI: 10.1017/S0954102003001275

Gas hydrate volume estimations on the South Shetland continental margin, Antarctic Peninsula

Y.K. JIN[1,*], M.W. LEE[2], Y. KIM[1], S.H. NAM[1] and K.J. KIM[1]

[1]*Korea Ocean Research and Development Institute, Ansan, PO Box 29, Seoul 425-600, Korea*
[2]*US Geological Survey, Denver Federal Center, Box 25046, MS939, Denver, CO 80225, USA*
**ykjin@kordi.re.kr*

Abstract: Multi-channel seismic data acquired on the South Shetland margin, northern Antarctic Peninsula, show that Bottom Simulating Reflectors (BSRs) are widespread in the area, implying large volumes of gas hydrates. In order to estimate the volume of gas hydrate in the area, interval velocities were determined using a 1-D velocity inversion method and porosities were deduced from their relationship with sub-bottom depth for terrigenous sediments. Because data such as well logs are not available, we made two baseline models for the velocities and porosities of non-gas hydrate-bearing sediments in the area, considering the velocity jump observed at the shallow sub-bottom depth due to joint contributions of gas hydrate and a shallow unconformity. The difference between the results of the two models is not significant. The parameters used to estimate the total volume of gas hydrate in the study area were 145 km of total length of BSRs identified on seismic profiles, 350 m thickness and 15 km width of gas hydrate-bearing sediments, and 6.3% of the average volume gas hydrate concentration (based on the second baseline model). Assuming that gas hydrates exist only where BSRs are observed, the total volume of gas hydrates along the seismic profiles in the area is about 4.8×10^{10} m3 (7.7×10^{12} m^3 volume of methane at standard temperature and pressure).

Received 8 February 2002, accepted 11 September 2002

Key words: baseline models, bottom simulating reflector, seismic data, unconformity, volume estimation

Introduction

Gas hydrates are ice-like crystalline solids composed of water molecules, with gas, commonly methane, encaged in a crystalline lattice. Gas hydrates form under low temperature and high pressure conditions when water is saturated with gas (Sloan 1998). They are stable in permafrost regions and at pressure-temperature conditions for seafloor below approximately 300–500 m water depth (Kvenvolden 1993).

Natural gas hydrates have increasingly attracted the attention of the scientific community mainly because of the vast amounts of methane that may be stored in gas hydrates, their potential role in climate change, and their possible interaction with seafloor stability. The global volume of methane contained in gas hydrate ranges from 10^{15} to 10^{17} m^3, which greatly exceeds the volumes of methane present in other forms (Kvenvolden 2000). Gas hydrates have been recognized from seismic reflection profiles, geochemical and geological studies worldwide (Deep Sea Drilling Program (DSDP) and Ocean Drilling Program (ODP)) (Kvenvolden & Lorenson 2001).

The typical signature of gas hydrates on seismic profiles is a high-amplitude reflection that approximately parallels the seafloor and deepens with increasing water depth, which is known as the gas hydrate 'bottom simulating reflector (BSR)' (Tucholke *et al.* 1977, Shipley *et al.* 1979). Gas hydrate BSRs are commonly associated with the base of a gas hydrate stability field and may represent the phase boundary between gas-hydrate-bearing sediments above and gas-charged or water-bearing sediments below. Pure gas hydrates have a seismic velocity in the range 3.3–3.8 km s^{-1} (Whalley 1980, Sloan 1998), much higher than normal oceanic sediments in the depth range of the

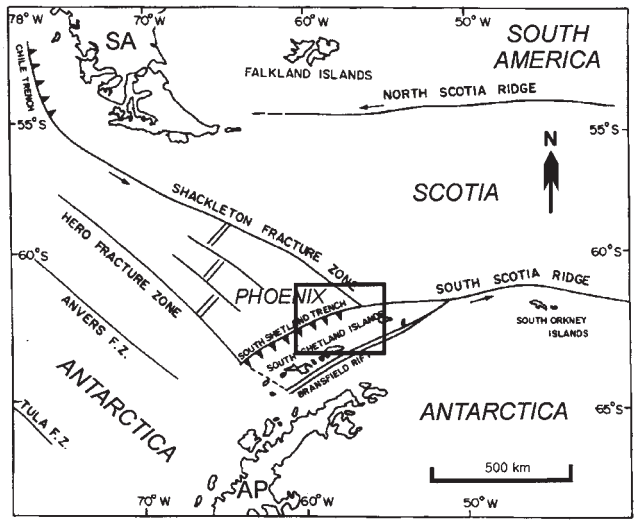

Fig. 1. Geological setting around the northern Antarctic Peninsula (modified from Jeffers & Anderson 1990). The box indicates the study area. AP = Antarctic Peninsula, SA = South America.

hydrate stability field. Filling the pore spaces of marine sediments above the phase boundary with gas hydrates causes the velocity to increase proportionally to the gas hydrate concentration (Lee *et al.* 1996, Jakobsen *et al.* 2000) whereas the presence of even a small amount of gas in the pore space below the phase boundary causes a dramatic decrease in seismic velocity (Domenico 1977). Hence the latter phase boundary has a high acoustic impedance contrast, giving rise to a strong seismic reflection with opposite polarity to the seafloor reflection. The BSR reflection amplitude depends on the degree of saturation of the sediments by gas hydrates above and by gas or water below, but is dominated by the free gas underneath the phase boundary.

Gas hydrate samples have been recovered from 19 regions in the world by deep drillings (DSDP and ODP) and coring in the oceans, and drilling in polar continental sediments (Kvenvolden & Lorenson 2001). These samples provide the most direct evidence for the global presence of gas hydrate.

In the Antarctic margin, BSRs on seismic profiles have been reported in four areas (Lodolo & Camerlenghi 2000). Among the areas, the BSRs on the South Shetland continental margin (Lodolo *et al.* 1993, Tinivella *et al.* 1998b) and Wilkes Land margin (Kvenvolden *et al.* 1987, Tanahashi *et al.* 1994) are known to be gas hydrate-related BSRs. The BSRs on the South Shetland continental margin have been clearly identified on seismic profiles as a high-amplitude, reverse polarity and nearly continuous reflections crossing sedimentary reflections (Lodolo *et al.* 1993, 1998, 2002, Tinivella *et al.* 1998a, Tinivella & Accaino 2000).

In this study, we analysed multichannel seismic reflection profiles to examine gas hydrate occurrences on the north-

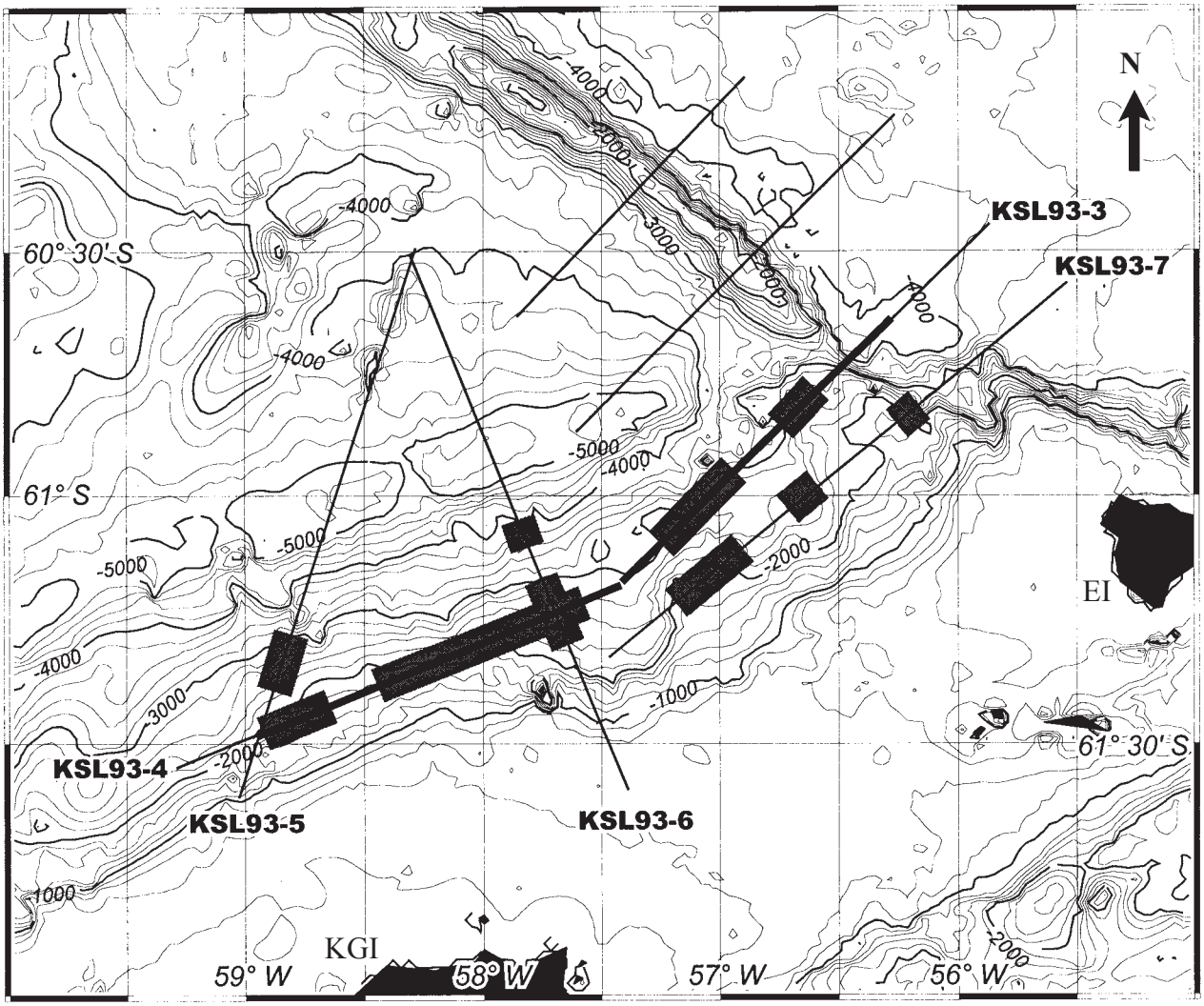

Fig. 2. Location of multichannel seismic lines overlaid on bathymetric contour map. Thick solid lines indicate the location of profiles of KSL93-3 and 4 shown in Fig. 3. Distribution of BSRs observed on the profiles is marked with grey rectangles. Bathymetry is derived from Smith & Sandwell (1997). Contour interval is 200 m. KGI =King George Island, EI = Elephant Island.

https://doi.org/10.1017/S0954102003001275 Published online by Cambridge University Press

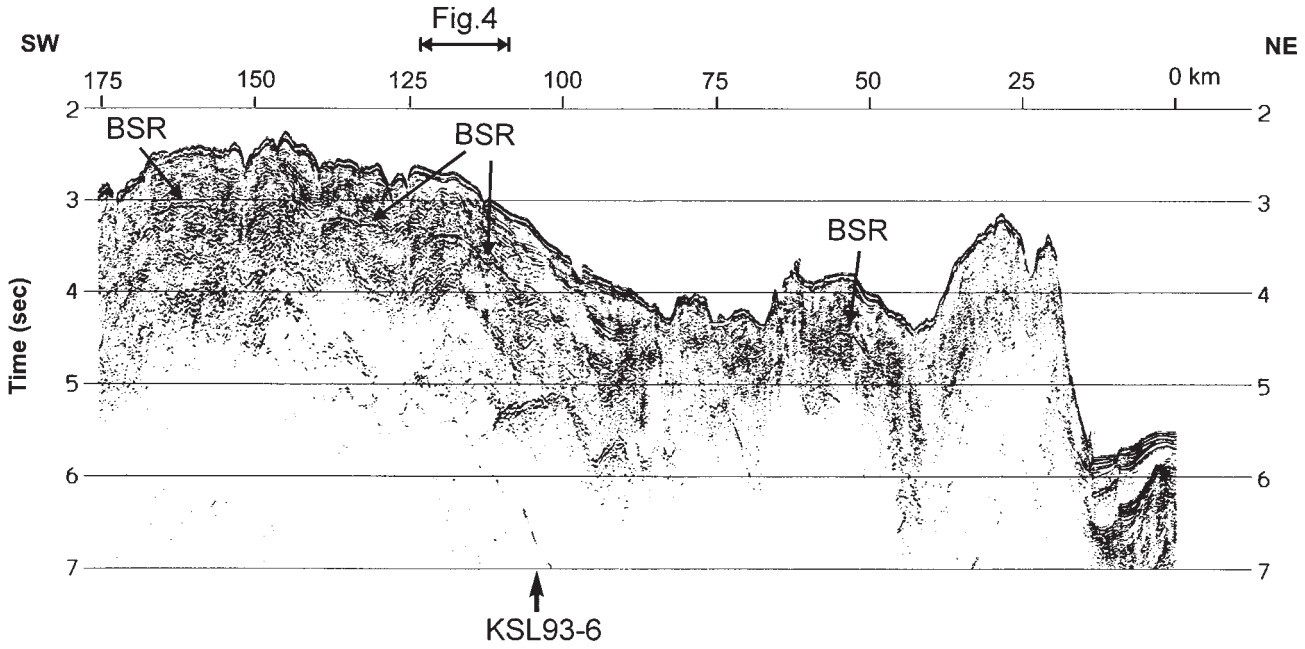

Fig. 3. Multichannel seismic profile of KSL93-3 and 4 show bottom simulating reflectors (BSRs) at about 600 ms two-way travel time beneath the seafloor. See Fig. 2 for location. The cross-over point with profile KSL93-6 is marked at the bottom of the figure.

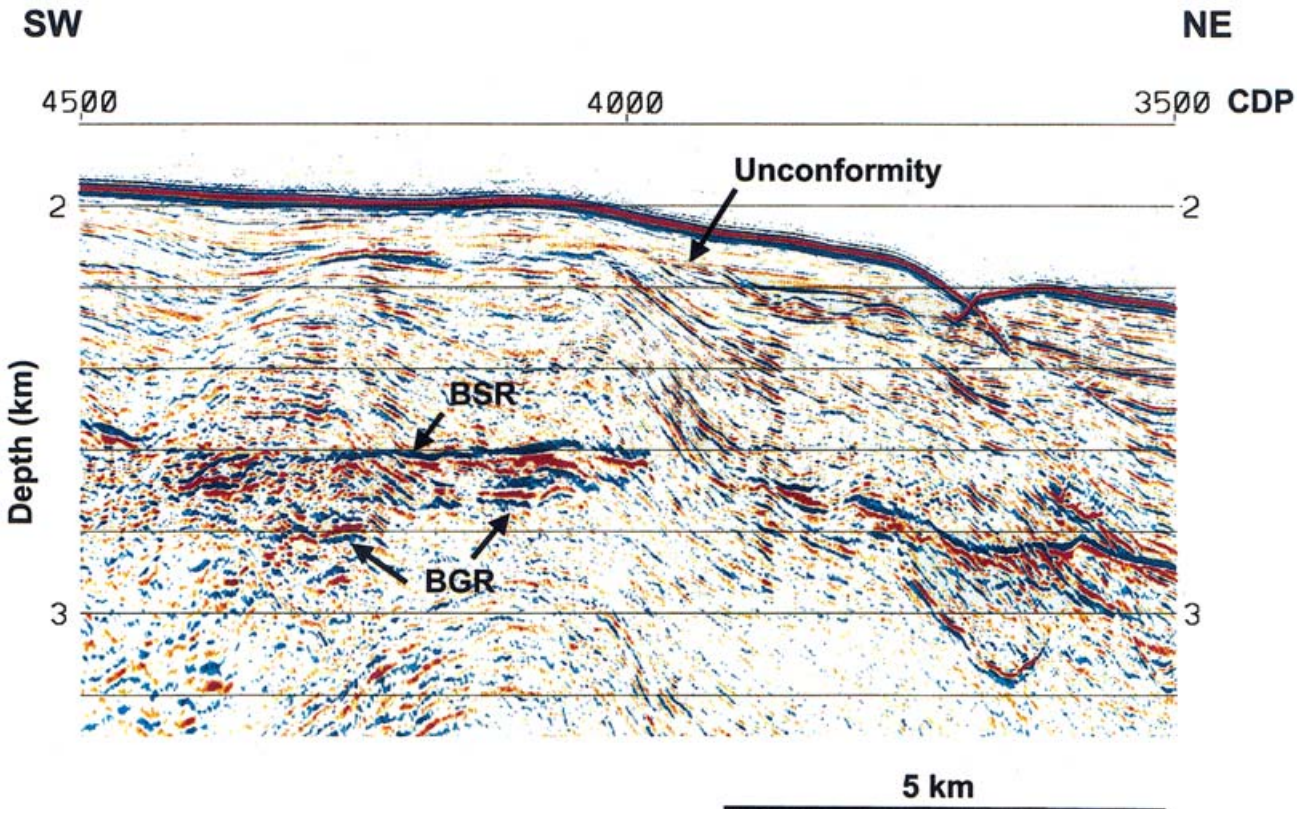

Fig. 4. Depth-converted seismic section of profile KSL93-4 showing well-developed BSRs, base of gas reflector (BGR), and an unconformity just beneath the seafloor. See Fig. 3 for location.

https://doi.org/10.1017/S0954102003001275 Published online by Cambridge University Press

eastern South Shetland continental margin, Antarctic Peninsula. Our results draw attention to the seismic characteristics of gas-hydrate-bearing sediments, the BSRs and the free gas zones below the BSRs. We estimate the volume of gas hydrate on the north-eastern South Shetland continental margin.

Geological setting

The South Shetland continental margin is located at the north-eastern tip of the Pacific margin of the Antarctic Peninsula. The Pacific margin of the Antarctic Peninsula has been an active margin since the break-up of Gondwana (Pankhurst 1982). During the Cenozoic, ridge-crest segments of the Antarctic–Phoenix spreading centre began to arrive at the Antarctic Peninsula margin. These arrivals moved progressively north-eastward along the margin. The last arrival of a ridge-crest segment took place directly south-west of the Hero Fracture Zone (HFZ) between 6.4 Ma and 3.3 Ma (Larter *et al.* 1997). Subduction stopped as each ridge-crest segment arrived and the entire margin south-west of the HFZ became passive (Barker 1982, Larter & Barker 1991). To the north-east of the HFZ, however, three segments of the Antarctic–Phoenix ridge remain seaward of the South Shetland margin (Fig. 1). Although spreading at the ridge ceased at about 4 Ma, shortening is considered to be active along the South Shetland Trench (SST) between the South Shetland continental block and the former Phoenix oceanic plate (Kim *et al.* 1995).

The South Shetland continental block is a tectonic block bounded by four major structures: to the north-east by the Shackleton Fracture Zone (SFZ), to the south-west by the HFZ, to the north-west by the SST, and to the south-east by Bransfield Strait (BS) (Fig. 1). BS is a marginal basin formed by recent extension between the South Shetland Islands (SSI) and the Antarctic Peninsula (Barker 1982, Gambôa & Maldonado 1990). The geometry of the SST, SSI and BS between the HFZ and the SFZ has led many scientists to interpret BS as a back-arc basin (Barker 1982, Larter & Barker 1991). Transtensional tectonics propagated from the plate boundary between the Scotia and Antarctic plates at the northern tip of the Antarctic Peninsula may also be contributing to extensional regime in BS (Barker & Austin 1994, Klepeis & Lawver 1996)

The study area is located in the complex tectonic environment of the north-eastern sector of the South Shetland continental margin. There is a triple junction where three major tectonic structures (the SFZ, the South Scotia Ridge, and the SST) meet (Fig. 1). The SFZ and the South Scotia Ridge are active transform systems forming the western and the southern boundaries of the Scotia plate with the Antarctic plate (Pelayo & Wiens 1989, Klepeis & Lawver 1996). The SST is a convergent boundary between the South Shetland continental block and the former Phoenix plate. The stress due to recent westward movement of the Scotia plate has caused strong deformation in the area around the triple junction (Klepeis & Lawver 1996, Kim *et al.* 1997, Jin *et al.* 2000).

Seismic data acquisition and processing

The Korean Ocean Research and Development Institute (KORDI) collected multichannel seismic (MCS) reflection data on the South Shetland continental margin on RV *Onnuri* cruise in the 1993 summer. The locations of MCS profiles used for this study are shown in Fig. 2. Data were acquired with a 2400 m long, 96-channel hydrophone streamer and a 16-airgun source with a total volume of 22.6 l. Shots were fired at a spacing of 50 m, giving 24-fold coverage. The data sampling rate was 4 ms.

In order to optimize the appearance and to carry out quantitative analysis for gas hydrate-related seismic characteristics (i.e. BSR), relative true amplitude processing with wavelet deconvolution was conducted. Wavelet deconvolution was performed by the variable norm deconvolution method (Gray 1979). A representative source

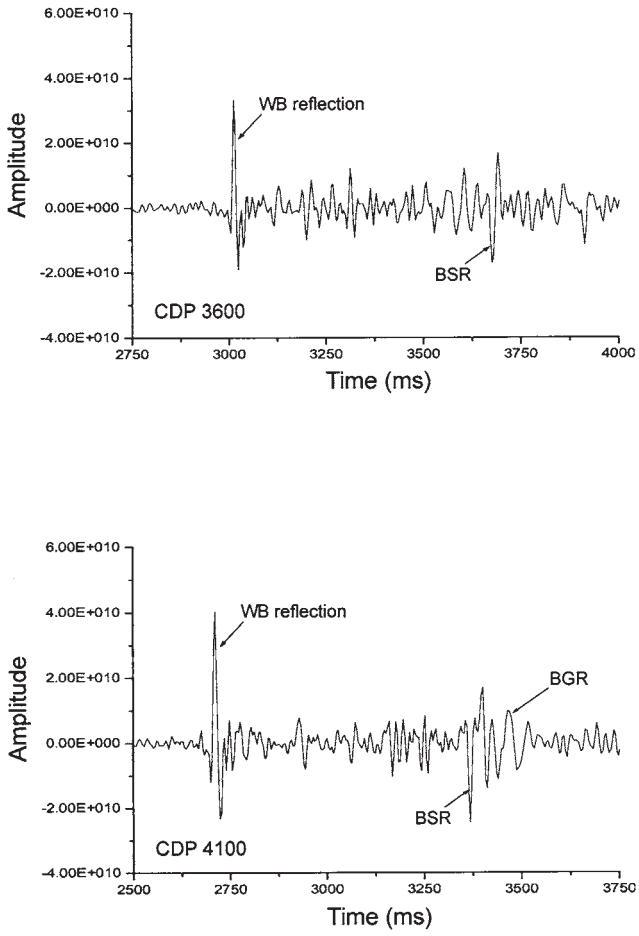

Fig. 5. Graphs showing detailed waveforms at CDP 3600 and CDP4100 in Fig. 4. BSRs in the graphs show high amplitude and opposite polarity to water bottom reflection.

https://doi.org/10.1017/S0954102003001275 Published online by Cambridge University Press

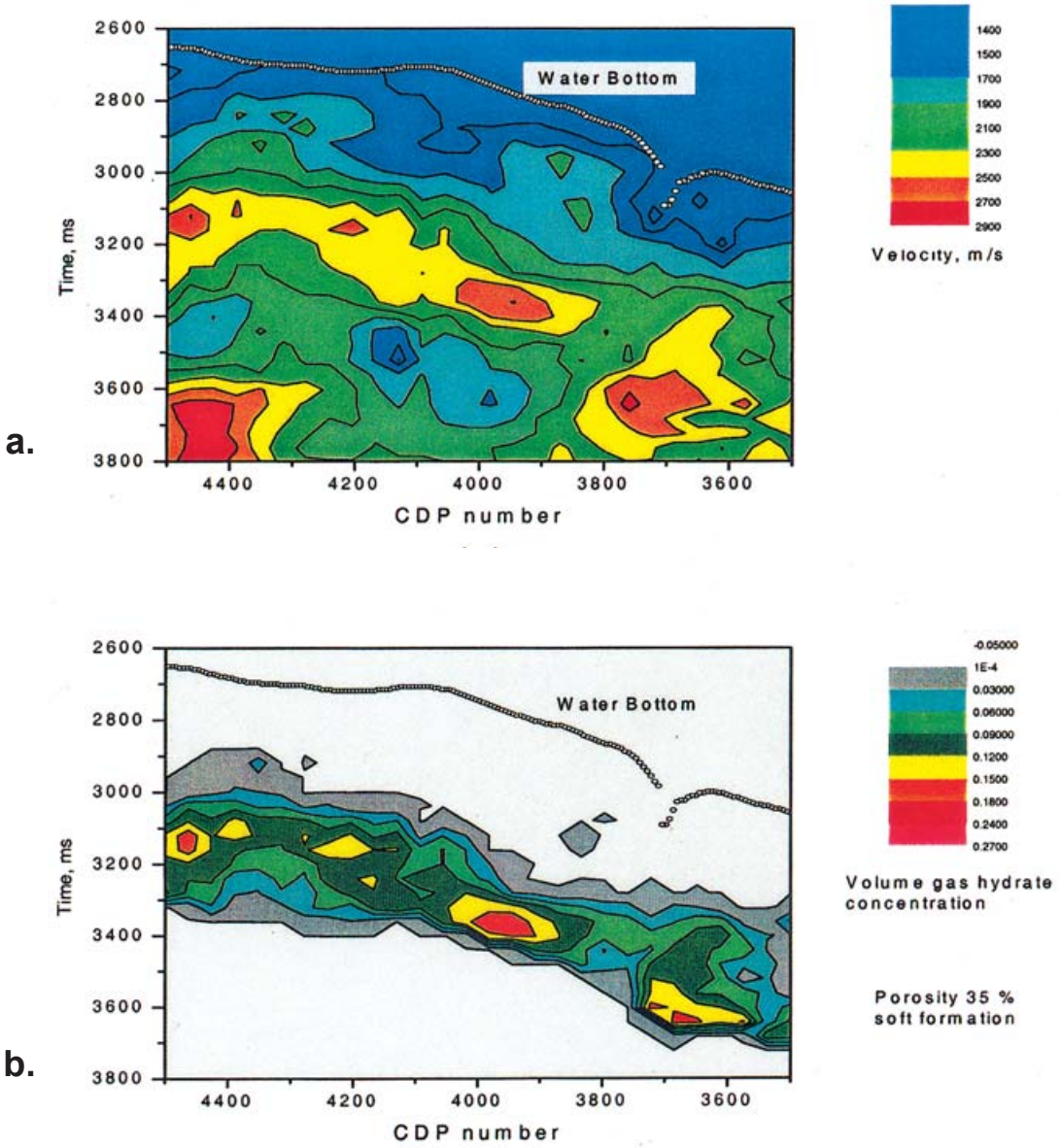

Fig. 6. a. Interval velocities between CDP 3500 and 4500 estimated from one-dimensional inversion of migrated seismic data. BSRs occurred at the sub-bottom time of about 600 ms are characterized by velocities higher than 2300 m s^{-1}, **b.** estimated volume of gas hydrates using a model with 10% reduction in porosity below an unconformity. See text for details. The highest volume gas hydrate concentration is about 18% near CDP 3700, 3900, and 4500.

signature in the area (at about 3 s two-way travel time (TTWT)) was derived, and an inverse filter was computed for and applied to each trace. Second-zero crossing predictive deconvolution was applied to compensate for the source signature variations caused by changes in airgun and streamer depths. Dip move-out (DMO) correction was applied to improve interval velocities.

BSR characteristics and distribution

On the north-eastern South Shetland margin, a remarkable feature on seismic profiles is the high-amplitude BSR approximately parallel to the seafloor (Fig. 3). The depth of the BSRs on profiles KSL93-3 and KSL93-4 is about 600 ms in TWTT beneath the seafloor. Local discontinuities of the BSRs on the profiles may be caused by structural discontinuities and disturbances at the base of gas hydrate stability field. Fig. 4 shows that the strong BSRs between CDP 3500 and 4500 cross dipping sedimentary layers.

Detailed waveforms for the BSRs at CDP 3600 and CDP 4100 are shown in Fig. 5. The BSRs have polarities opposite to the water-bottom reflection, indicating that the reflections mark the boundary between a high-impedance layer and a low-impedance layer. The reflection coefficients calculated

https://doi.org/10.1017/S0954102003001275 Published online by Cambridge University Press

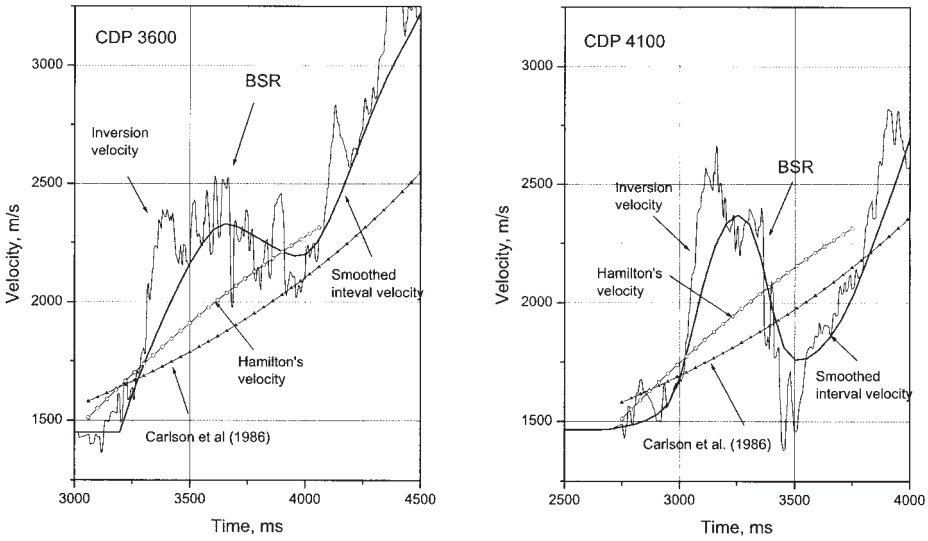

Fig. 7. Graphs showing detailed velocity inversion results at CDP 3600 and 4100.

for the BSRs are about -0.2. This value is similar to that of the strong BSR in the Blake Ridge region off the south-eastern United States (Lee *et al.* 1994).

We can see another distinct reflection subparallel to and beneath the BSR between CDP 4050 and CDP 4400 in Fig. 4. The depth of this reflection beneath the BSR varies from about 120 m to 200 m. As shown in Fig. 4, the polarity of the reflection is a peak-trough (red-blue), the same as the seafloor reflection and opposite to the polarity of the BSR, which indicates that the reflection occurs at the boundary between an upper low-impedance layer and a lower high-impedance layer. The reflector is interpreted as a base of gas reflector (BGR), and the existence of the BGR has previously been reported in the South Shetland margin (Tinivella *et al.* 1998b, Lodolo *et al.* 2002). Figure 5 shows the strong amplitude of the BGR at CDP 4100 where it is well developed, but no distinct amplitude corresponding to the BGR at CDP 3600.

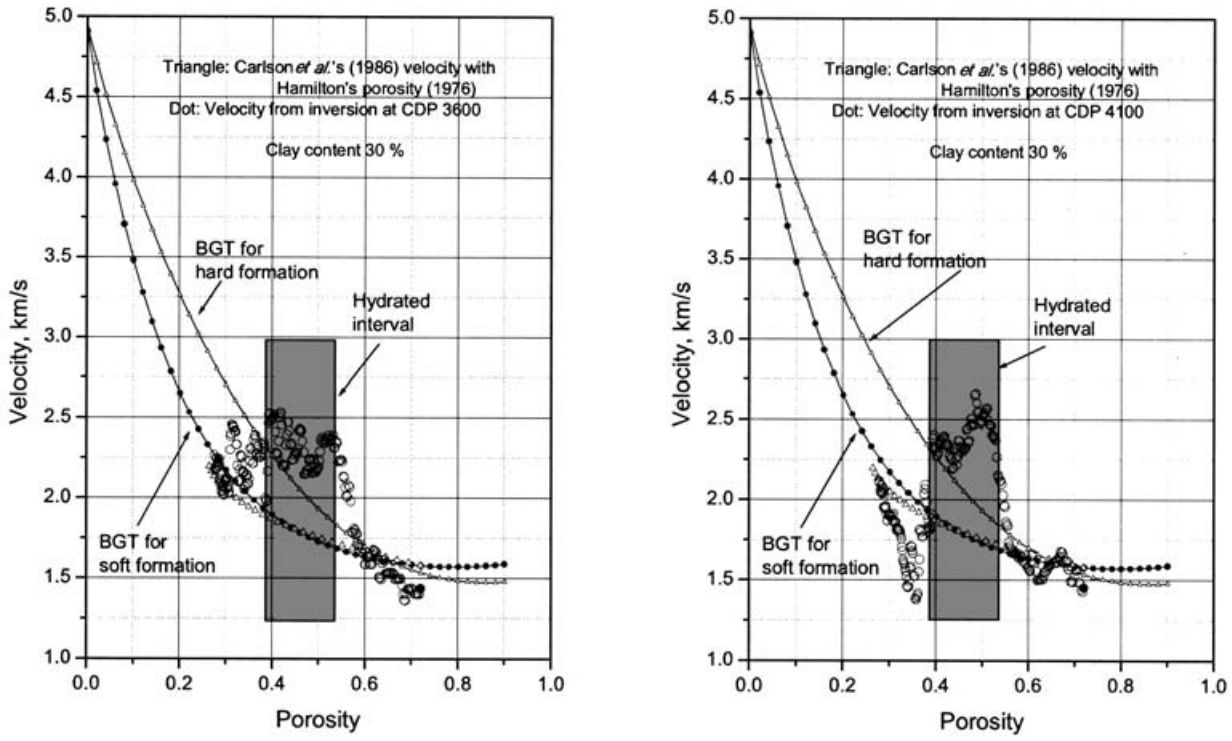

Fig. 8. Graphs showing the velocities with respect to porosities at CDP 3500 and CDP 4100 for sub-bottom depth less than 1000 m. For a reference, velocities from Biot-Gassman theory (BGT) for soft and hard formations, and from Carlson *et al.* (1986) are also shown. Shaded regions in the graphs indicate the hydrated depth intervals in sediments.

https://doi.org/10.1017/S0954102003001275 Published online by Cambridge University Press

We identified the BSRs on MCS profiles KSL93-3, 4, 5, 6, and 7. The distribution of the BSRs on the profiles is shown in Fig. 2. The BSR is widespread in the study area, more so on profiles parallel to the margin (KSL93-3, 4, and 7) than on profiles across the margin (KSL93-5 and 6).

Interval velocities and porosities

Interval velocities were estimated from one-dimensional inversion of migrated seismic data. In this paper, one-dimensional inversion is the same as the processing method of calculating synthetic sonic logs (Lindseth 1979). It was performed using 'Constrained Impedance Inversion' in the seismic processing software package ProMAX®. A sparse reflectivity series is computed (e.g. Oldenburg *et al.* 1983). The sparse reflectivity series contains information about the high-frequency component of impedance. Because the seismic data are band-limited, the low-frequency component of the impedance cannot be estimated from the inversion. Usually the low-frequency impedance information is obtained from well logs (Lindseth 1979) or from seismic data using move-out velocity analysis (Lavergne & Willm 1977). In this study, the low-frequency component of impedance is derived from the interval velocities obtained by the migration velocity analysis. As indicated in the data acquisition, the far offset of seismic data is 2.4 km. This offset distance is insufficient to provide accurate interval velocities for water depths exceeding 2 km. At these depths, the emphasis is on variation of interval velocities in the gas-hydrate-bearing sediments.

From the water bottom to the BSR level, interval velocities vary between 1500 and 2700 m s^{-1} and generally increase with increasing depth (Fig. 6a). Low velocities from 1500 to 1700 m s^{-1} between CDP 4000 and 4200 underneath high velocities ranging from 2300 to 2700 m s^{-1} indicate the presence of free gas.

Figure 7 shows examples of detailed velocity inversion results at CDP 3600 and at CDP 4100. For comparison, the velocities predicted by Hamilton (1979) and by Carlson *et al.* (1986) are also shown. Generally, velocities by Hamilton (1979) are higher than those by Carlson *et al.* (1986) when the sub-bottom time is greater than about 150 ms. Our inversion results show a significant velocity increase beneath about 200 ms in sub-bottom depth, and a velocity drop at the BSR due to the presence of underlying free gas. At CDP 4100 where the BGR is well developed in the seismic section as shown in Fig. 4, the velocity contrast between the hydrate-bearing sediments and the sediments having free gas is up to 800 m s^{-1}. The velocity contrast at CDP 3600 where the BGR is not clear is rather subtle.

Hamilton (1976) presented a relationship between porosity and sub-bottom depth for terrigenous sediments. Using Hamilton's relationship, velocities versus porosities at CDP 3600 and at CDP 4100 for sub-bottom depths less than 1000 m are shown in Fig. 8 as large dots. For reference, velocities predicted from the Biot-Gassmann theory (BGT) for soft (unconsolidated) and hard (consolidated) formations (Lee 2002), and from Carlson *et al.* (1986) are also shown. Appendix A presents a summary for BGT. The parameters are shown in Table I and a 30% clay volume content in the sediment's matrix is assumed. A change in clay content would contribute a significant change in sediment velocity. Velocities by Carlson *et al.* (1986) are very close to those predicted from BGT for soft formations except that BGT predicts slightly higher velocities when the porosities are less than about 40%.

For a porosity of about 55%, a large velocity change is observed (from 1700 to 2400 m s^{-1} at CDP 3600 and from 1700 to 2700 m s^{-1} at CDP 4100) as shown in Fig. 8. In the shaded region in Fig. 8, velocities are higher than those predicted from BGT and Carlson *et al.* (1986), implying that a significant gas hydrate is present in this interval. The lower than predicted velocities at CDP 4100 for porosities less than about 40% indicate the presence of free gas.

Table I. Elastic constants used for baseline velocity models and for velocities of gas-hydrate-bearing sediments.

Definition	Symbols	Values	Sources
Shear modulus of quartz	(*Gpa*)	45	Helgerud *et al.* (1999)
Bulk modulus of quartz	(*Gpa*)	36	Helgerud *et al.* (1999)
Shear modulus of clay	(*Gpa*)	6.85	Helgerud *et al.* (1999)
Bulk modulus of clay	(*Gpa*)	20.9	Helgerud *et al.* (1999)
Shear modulus of hydrate	(*Gpa*)	2.54	*Sloan (1998)
Bulk modulus of hydrate	(*Gpa*)	6.41	*Sloan (1998)
Bulk modulus of water	(*Gpa*)	2.29	
Density of quartz	(g cm^{-3})	2.65	Helgerud *et al.* (1999)
Density of clay	(g cm^{-3})	2.58	Helgerud *et al.* (1999)
Density of hydrate	(g cm^{-3})	0.91	Sloan (1998)

*The shear and bulk moduli are computed from the P-wave and S-wave velocities with the density given in Sloan (1998) for structure I type hydrate.

Baseline models for gas-hydrate-bearing sediments

Because filling the pore space with gas hydrates with higher elastic velocity increases the elastic velocity of sediments, the amount of velocity increase in gas-hydrate-bearing sediments directly corresponds to the amount of gas hydrates in sediment. Therefore, porosities and velocities of non-gas-hydrate-bearing sediments (baseline) should be known in order to estimate the amount of gas hydrate in sediments from the velocity increment of sediments.

It is difficult to determine the baseline in this study area, because there are no available well logs and there is a significant geological complexity. ODP Legs 113 (Weddell Sea) and 178 (south-western Antarctic Peninsula) in Antarctica are located too far from the study area, especially as the northern Antarctic Peninsula is in a highly complex tectonic environment. It is also difficult to get a baseline from seismic data alone because absence of a BSR does not

https://doi.org/10.1017/S0954102003001275 Published online by Cambridge University Press

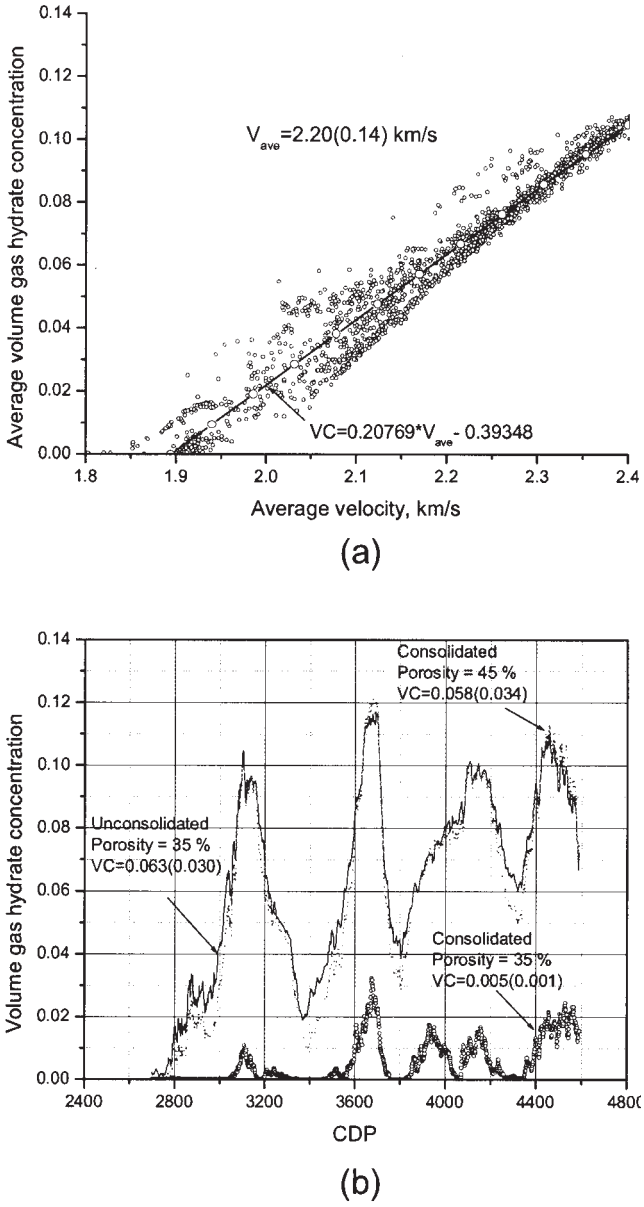

Fig. 9. a. Average velocities for the gas hydrate bearing depth (330 to 650 ms sub-bottom time) for all CDPs from 2700 to 4500, **b.** volume gas hydrate concentrations (VC) for the each baseline model.

necessarily imply the absence of hydrates in the sediments (ODP Leg 164, Paull *et al.* 2000).

In this study, we used the reference velocities for normally compacted terrigenous sediments (Hamilton 1979) and the porosities derived from the relationship between the porosity and sub-bottom depth for terrigeneous sediments proposed by Hamilton (1976) as a baseline. Tinivella *et al.* (1998a, 1998b) mentioned that the baseline for normally compacted terrigenous sediments is almost consistent with the velocity profile for non-gas-hydrate-bearing sediments in the northern Antarctic Peninsula region.

However, the seismic velocities determined from our data (Fig. 7) indicate a large velocity jump (from 1700 to 2400 m s^{-1} at CDP 3600 and from 1700 to 2700 m s^{-1} at CDP 4100) at about 100 to 200 ms in TWTT below the sea floor. If the velocity jump is entirely due to gas hydrates, pore space in the sediments should be completely filled with gas hydrate. As mentioned earlier, the north-eastern Antarctic Peninsula region is a complex tectonic environment (Fig. 4). Furthermore, on the Antarctic Peninsula margin, the outer shelf sediments directly below the seafloor are known to have high seismic velocities in excess of 2000 m s^{-1} (Larter *et al.* 1997). Thus we need to distinguish between the contributions of gas hydrates and geology to the velocity increase.

In Fig. 4, we can see an unconformity as a reflector that clearly truncates underlying dipping sedimentary reflections beneath the seafloor. The depth of the velocity jump observed in this study is close to that of the shallow unconformity. The existence of the shallow unconformity complicates in determining the baseline of non-hydrate-bearing sediments. The velocity jump may be partly due to the unconformity and partly due to the gas hydrate. To assess the contribution of the unconformity to the velocity jump, we have proposed two baseline models.

Model 1 assumes that the porosities of the gas hydrate sediments follow the equation proposed by Hamilton (1976) and that the velocity jump is partly due to consolidation. Fig. 8 indicates that the porosity of the gas-hydrate-bearing interval varies between 40% and 50%. We use an average porosity for the gas-hydrate-bearing sediments of 45% and the baseline velocity is predicted from BGT using the Biot coefficient for hard formations.

Model 2 assumes that the *in situ* porosity is less than that predicted by the Hamilton's equation by about 10% below the unconformity, but that the sediments are unconsolidated (soft formation). The 10% reduction compensates for the burial history of the sediments under the unconformity and corresponds to an increase velocity about 200 m s^{-1}. Therefore in this model, we use an average porosity of gas-hydrate-bearing sediments of 35% and the baseline velocity is predicted from BGT using the Biot coefficient for the soft formation.

Estimation of gas hydrate amount

From the interval velocities for gas-hydrate-bearing sediments and the baseline models for non-gas-hydrate-bearing sediments, we estimate the amount of gas hydrate in gas-hydrate-bearing sediments using BGT.

Estimated gas hydrate amounts for Model 2 between CDP 3500 to CDP 4500 are shown in Fig. 6b. The highest volume gas hydrate concentration (porosity times the gas hydrate concentration in the pore space) is about 18% near CDP 3700, 3900, and 4500. Because the assumed porosity

https://doi.org/10.1017/S0954102003001275 Published online by Cambridge University Press

in this model is 35%, the highest gas hydrate concentration in the pore space is about 50%.

The average velocities for the gas-hydrate-bearing sediment interval (200 to 640 ms sub-bottom time) and the volume gas hydrate concentrations for two baseline models are shown in Fig. 9a & b, respectively. To a first order approximation, the average velocity is linearly related to the average volume gas hydrate concentration, so average velocities can be used for a quick estimation of gas hydrates. The average velocity for all CDPs between CDP 2700 and 4500 in Fig. 4 is about 2.08 km s^{-1} and the average volume gas hydrate concentrations are 5.83.4% for Model 1 and 6.33.0% for Model 2 (Fig. 9b). The error is a standard deviation of the gas hydrate estimations from all CDPs. This only provides the uncertainty of the average calculated under the assumption that all parameters and assumption used in the study are correct. The difference between the results of two models is not significant. This estimation is comparable with those of other researches in the study area, 5% of volume concentration from Tinivella & Carcione (2001), 5–20% of the pore space from Tinivella *et al.* (1998b).

In an extreme model where both the assumption of consolidation and of 10% reduction in porosity apply, the average volume gas hydrates concentration goes down to 0.5% as shown in Fig. 9b, indicating nearly non-gas-hydrate-bearing sediments. This model may provide the minimum volume estimate of gas hydrate in the study area. However, well-developed BSRs and BGRs are not likely to occur with such very low concentrations of gas hydrate.

The total amount of gas hydrate in the study area is estimated by summing each individual amount for the area showing the BSR. Besides the average volume concentration of gas hydrate, the parameters needed in calculating the amount of gas hydrate are thickness, length (along the seismic profiles), and width (across the profiles) of the gas-hydrate-bearing layers. Length was measured directly from the BSR length on the MCS profiles. Thickness was determined from the interval that has the velocity jump as the upper boundary and the BSR as the lower boundary. The average thickness used in this study is 350 m. Determination of width (that is, the across-profile extent) of gas hydrate layers in this study is not rigorous. With our 2-D seismic lines, it is difficult to get information on the across-profile width of the gas hydrate layers. We have two cross-over points. The point between profiles KSL93-4 and 6 is located at the place where the BSR is well developed (Fig. 3), whereas the other point between profiles KSL93-4 and 5 is located at a non-BSR area. At the former point, the lengths of the BSRs are 45 km on profile KSL93-4 and 15 km on profile KSL93-6, respectively. As mentioned earlier, the BSRs are probably longer and more continuous along the margin than across the margin. A possible interpretation is that geology and water depth are relatively uniform along the margin but are highly variable down the steep continental slope. We used 15 km as an average width of gas hydrate layers on the MCS profiles. The BSRs on the sub-parallel profiles KSL93-3 and 7 shown along the same latitudes are likely to be connected to each other (Fig. 2). Another seismic profile presented by Lodolo & Camerlenghi (2000), sub-parallel to and south-east of profile KSL93-7, also shows well-developed BSRs with high continuity along the entire profile. This indicates that the BSRs are widespread in the study area and that the 15 km average width used in this study is not excessive.

Assuming that gas hydrates exist only where BSRs are observed and given the above parameters for length, thickness, width and average volume gas hydrate concentration, the total volume of gas hydrates calculated along the seismic lines in the area is estimated about 4.8×10^{10} m^3 (7.7×10^{12} m^3 volume of methane at standard temperature and pressure). Previous studies (Tinivella *et al.* 1998b, Tinivella & Accaino 2000, Tinivella & Carcione 2001, Lodolo *et al.* 2002) also presented the distribution and concentration of gas hydrates in the South Shetland margin. Most recently, Lodolo *et al.* (2002) obtained an amount of 2.3×10^{12} m^3 volume of methane from gas hydrate layer and 5.9×10^{10} m^3 for free gas below the BSR in the area. Despite using different inversion methods, our results show reasonable agreement with those of Lodolo *et al.*

According to Collett (2000), the volumes of methane in gas hydrate and associated gas are $57\sim80\times10^{12}$ m^3 for the Blake Ridge and 50×10^{12} m^3 for the Nankai Trough, respectively. Considering the broad area outside the coverage of our seismic lines, the volume of gas hydrate on the north-eastern South Shetland continental margin is likely to be higher than that estimated in this study, which may be comparable to the above well-known gas hydrates regions in the world.

There are positive (to overestimate) and negative (to underestimate) factors for the estimation of the total volume of gas hydrate in this study. Firstly, we calculate the volume only at the place where the BSRs are observed. This may not be true given the recent discovery of gas-hydrate-bearing sediments at the Blake Ridge during ODP leg 164 (Paull *et al.* 2000), where no BSR observed in the seismic section. Therefore, the estimation of total volume of gas hydrate based only on the BSR areas is a conservative one. Secondly, we use an average volume gas hydrate concentration of 6.3% based on the well-developed BSR between CDPs from 2700 to 4500 in Fig. 4 along profile KSL93-4. Weaker BSRs on the same and other profiles would represent a concentration lower than 6.3%.

Another controlling factor in estimating amounts of gas hydrate is the velocity anisotropy of the sediment. Based on waveform inversion of wide-angle P-wave velocity and zero offset vertical seismic profiling data at the Blake Ridge, Holbrook (2001) concluded that the P-wave velocities of wide-angle data are about 6% higher than downhole velocities, due to anisotropy of horizontally

https://doi.org/10.1017/S0954102003001275 Published online by Cambridge University Press

layered sediments. If the same degree of anisotropy and the second baseline model are assumed in this area, the volume of gas hydrate concentrate would be reduced to 4 ± 2%, which is about a 35% reduction of the gas hydrate amounts. Because the geological setting of the study area is quite different from that of the Blake Ridge, it is not clear whether velocity anisotropy is relevant in this area. However, this example emphasized that velocity anisotropy may significantly affect estimates of gas hydrate amounts.

Conclusion

The South Shetland margin in the northern Antarctic Peninsula is the only active continental margin around the Antarctic. Recently, well-developed BSRs have been observed on seismic profiles. Reprocessed multichannel seismic data were optimized for hydrate-related seismic characteristics and used to estimate the amounts of gas hydrate on the north-eastern South Shetland continental margin.

For a baseline in estimating amount of the gas hydrates, interval velocities were determined by 1-D velocity inversion and porosities were deduced from their relationship with respect to the sub-bottom depth for terrigenous sediments. The velocity jump observed at the shallow sub-bottom depth of about 200 ms is caused by both gas hydrate beneath and the shallow unconformity at this depth. As there are no available well logs, we made two baseline models for the velocities and porosities of non-gas-hydrate-bearing sediments depending on the significance of the unconformity. The first model assumes that the velocity increase is partly due to consolidated sediment (hard formation) beneath the unconformity. The second model assumes that the porosity is reduced by 10% beneath the unconformity but that the sediments are unconsolidated (soft formation). The average volume gas hydrate concentration calculated is 5.8 ± 3% for the first model and 6.3 ± 3% for the second model. The difference between the results from two models is not significant.

The total length of the BSRs identified on all MCS profiles used in the study is about 145 km. Assuming a 350 m total thickness, a 15 km width along the seismic profile, and a 6.3% an average volume gas hydrate concentration (based on the baseline Model 2), the calculated total volume of gas hydrate along the seismic profiles in the area is about 4.8×10^{10} m^3 (7.7×10^{12} m^3 in a volume of methane at standard condition). Considering the broad area outside the coverage of our seismic lines, the amounts of gas hydrate on the north-eastern South Shetland continental margin may be comparable to well-known gas hydrates regions like the Blake Ridge ($57\sim80\times10^{12}$ m^3) and the Nankai Trough (50×10^{12} m^3)

Acknowledgements

We thank the scientists and technicians participating in the 1992/1993 cruise during data acquisition. The work was supported by the Ministry of Maritime Affairs and Fisheries of Korea under grant PM15800, and also significantly funded by KORDI under grant PP02103. Discussions with Timothy Collett during this study are very much appreciated. Our appreciation is also extended to the Geophysics group members for their technical support and assistance during Jin's postdoctoral fellowship program at the USGS in Denver. The paper was greatly improved by through comments and suggestions from Angelo Camerlenghi, Umberta Tinivella, Lieve Vanneste, and an anonymous reviewer.

References

Barker, P.F. 1982. The Cenozoic subduction history of the Pacific margin of the Antarctic Peninsula: ridge crest–trench interactions. *Journal of the Geological Society of London*, **139**, 787–801.

Barker, D.H.N. & Austin Jr, J.A. 1994. Crustal diaprism in Bransfield Strait, West Antarctica: evidence for distributed extension in marginal-basin formation. *Geology*, **22**, 657–660.

Carlson, R.L., Gangi, A.F. & Snow, K.R. 1986. Empirical reflection travel time versus depth and velocity versus depth functions for the deep-sea sediment column. *Journal of Geophysical Research*, **91**, 8249–8266.

Collett, T.S. 2000. Natural gas hydrates as a potential energy resource. *In* Max, M.D., *ed. Natural gas hydrate in oceanic and permafrost environments*. Dordrecht: Kluwer, 123–136.

Domenico, S.N. 1977. Elastic properties of unconsolidated porous sand reservoirs, *Geophysics*, **42**, 1339–1368.

Gambôa, L.A. & Maldonado, R. 1990. Geophysical investigations in the Bransfield Strait and in the Bellinghausen Sea-Antarctica. *In* St John, B., *ed. Antarctica as an exploration frontier - hydrocarbon potential, geology, and hazards*. *American Association of Petroleum Geologists Studies in Geology*, No. 31, 127–141.

Gray, W.C. 1979. *Variable norm deconvolution*. PhD thesis, Stanford University, CA, 101 pp. [Unpublished.]

Hamilton, E.L. 1976. Variation of density and porosity with depth in deep sea sediments. *Journal of Sedimentary Petrology*, **46**, 280–300.

Hamilton, E.L. 1979. Sound velocity gradients in marine sediments. *Journal of Acoustic Society of America*, **65**, 909–922.

Helgerud, M.B., Dvorkin, J., Nur, A., Sakai, A. & Collett, T.S. 1999. Elastic-wave velocity in marine sediments with gas hydrates: effective medium modeling. *Geophysical Research Letters*, **26**, 2021–2024.

Hill, R. 1952. The elastic behaviour of crystalline aggregate. *Proceeding of Physical Society of London*, **A65**, 349–354.

Holbrook, W.S. 2001. Seismic studies of the Blake Ridge: Implications for hydrate distribution, methane expulsion, and free gas dynamics. *In* Paull, C.K. & Dillon, W.P., *eds*. *Natural gas hydrate: occurrence, distribution, and detection*. *Geophysical Monograph Series, American Geophysical Union*, No. 124, 235–256.

Jakobson, M., Hudson, J.A., Minshull, T.A. & Singh, S.C. 2000. Elastic properties of hydrate-bearing-sediments using effective medium theory. *Journal of Geophysical Research*, **105**, 561–578.

Jeffers, J.D. & Anderson, J.B. 1990. Sequence stratigraphy of the Bransfield Basin, Antarctica, implication for tectonic history and hydrocarbon potential. *In* St John, B., *ed*. *Antarctica as an exploration frontier-hydrocarbon potential, geology, and hazards. American Association of Petroleum Geologists Studies in Geology*, No. 31, 13–29.

Jin, Y.K., Kim, Y., Nam, S.H. & Kim, K.J. 2000. Morphotectectic variation of the Shackleton Fracture Zone around the Antarctic–Scotia plate boundary off the northern Antarctic Peninsula. *Korean Journal of Geophysics*, **3**, 210–218.

Kim, Y., Jin, Y.K. & Nam, S.H. 1997. Crustal structure of the Shackleton Fracture Zone in the southwestern Scotia Sea, *In* Ricci, C.A., *ed*. *The Antarctic Region: geological evolution and process*. Siena: Terra Antartica Publications, 661–667.

Kim, Y., Kim, H.-S., Larter, R.D., Camerlenghi, A., Gambôa, L.A.P. & Rudowski, S. 1995. Tectonic deformation in the upper crust and sediments at the South Shetland Trench. *Antarctic Research Series*, **68**, 157–166.

Klepeis, K.A. & Lawver, L.A. 1996. Tectonics of the Antarctic–Scotia plate boundary near Elephant and Clarence islands, West Antarctica. *Journal of Geophysical Research*, **89**, 20211–20231.

Krief, M., Garta, J., Stellingwerff, J. & Ventre, J. 1990. A petrophysical interpretation using the velocities of P and S waves (full waveform sonic). *The Log Analyst*, **31**, 355–369.

Kvenvolden, K.A. 1993. A primer on gas hydrates: the future of energy gases. *US Geological Survey Professional Paper*, No. 1570, 279–291.

Kvenvolden, K.A. 2000. Natural gas hydrate: Introduction and history of discovery. *In* Max, M.D., *ed*. *Natural gas hydrate in oceanic and permafrost environments*. Dordrecht: Kluwer, 9–16.

Kvenvolden, K.A., Golan-Bac, M. & Rapp, J.B. 1987. Hydrocarbon geochemistry of sediments offshore from Antarctica: Wilkes Land continental margin. *CircumPacific Council for Energy and Mineral Resources*, *Earth Science Series*, **5A**, 205–213.

Kvenvolden, K.A. & Lorenson, T.D. 2001. The global occurrence of natural gas hydrate, *In* Paull, C.K. & Dillon, W.P., *eds*. *Natural gas hydrate: occurrence, distribution, and detection*. *Geophysical Monograph Series, American Geophysical Union*, No. 124, 3–18.

Larter, R.D. & Barker, P.F. 1989. Seismic stratigraphy of the Antarctic Peninsula Pacific margin: a record of Pliocene–Pleistocene ice volume and palaeoclimate. *Geology*, **17**, 731–734.

Larter, R.D., Rebesco, M., Vanneste, L.E., Gambôa, L.A.P., Barker, P.F. 1997. Cenozoic tectonic, sedimentary and glacial history of the continental shelf west of Graham Land, Antarctic Peninsula. *Antarctic Research Series*, **71**, 1–27.

Lee, M.W. 2002. Biot-Gassmann theory for velocities of gas hydrate-bearing sediments. *Geophysics*, **67**, 1711–1719.

Lee, M.W., Hutchinson, D.R., Agena, W.F., Dillon, W.P., Miller, J.J. & Swift, B.A. 1994. Seismic character of gas hydrates on the southeastern US continental margin. *Marine Geophysical Researches*, **16**, 163–184.

Lee, M.W., Hutchinson, D.R., Collett, T.S. & Dillon, W.P. 1996. Seismic velocities for hydrate-bearing sediments using a weighted equation. *Journal of Geophysical Research*, **101**, 20347–20359.

Lavergne, M. & Willm, C. 1977. Inversion of seismograms and pseudo velocity logs. *Geophysical Prospecting*, **25**, 231–250.

Lindseth, R.O. 1979. Synthetic sonic logs- a process for stratigraphic interpretation. *Geophysics*, **44**, 3–26.

Lodolo, E., Camerlenghi, A. & Brancolini, G. 1993. A bottom simulating reflection on the South Shetland margin, Antarctic Peninsula. *Antarctic Science*, **5**, 207–210.

Lodolo, E. & Camerlenghi, A. 2000. The occurrence of BSRs on the Antarctic margin, *In* Max, M.D., *ed*. *Natural gas hydrate in oceanic and permafrost environments*. Dordrecht: Kluwer Academic Publishers, 199–212.

Lodolo, E., Camerlenghi, A., Madrussani, G., Tinivella, U. & Rossi, G. 2002. Assessment of gas hydrate and free gas distribution on the South Shetland margin (Antarctica) based on multichannel seismic reflection data. *Geophysical Journal International*, **148**, 103–119.

Lodolo, E., Tinivella, U., Pellis, G. & RV OGS-Explora Party. 1998. Seismic investigation of Bottom Simulating Reflectors on the South Shetland margin. *Terra Antarctica Report*, **2**, 71–74.

Oldenburg, D.W., Scheuer, T. & Levy, S. 1983. Recovery of the acoustic impedance from reflection seismograms. *Geophysics*, **48**, 1318–1337.

Pankhurst, R.J. 1982. Rb–Sr geochronogy of Graham Land, Antarctica. *Journal of the Geological Society London*, **139**, 701–711.

Paull, C.K., Matsumoto, R., Wallace, P.J & Dillion, P.J., eds. 2000. *Proceedings of the Ocean Drilling Program*, *Scientific Results*, **164**.

Pelayo, A.M. & Wiens, D.A. 1989. Seismotectonis and relative plate motion in the Scotia Sea region. *Journal of Geophysical Research*, **94**, 7293–7320.

Raymer, L.L., Hunt, E.R. & Gardner, J.S. 1980. An improved sonic transit time to porosity transform. *21st Annual SPWLA Logging Symposium Transactions, Paper P.*

Shipley, T.H., Houston, M.H., Buffler, R.T., Shaub, F.J., McMillen, K.J., Ladd, J.W. & Worzel, J.L. 1979. Seismic evidence for widespread possible gas hydrate horizons on continental slopes and rises. *American Association of Petroleum Geologists Bulletin*, **63**, 2204–2213.

Smith, W.H.F. & Sandwell, D.T. 1997. Global sea floor topography from satellite altimetry and ship depth sounding. *Science*, **277**, 1956–1962.

Sloan, E.D. 1998. *Clathrate hydrate of natural gases*. New York: Marcel Dekker, 705 pp.

Tanahashi, M., Eittreim, S. & Wannesson, J. 1994. Seismic stratigraphic sequences of the Wilkes Land margin. *Terra Antarctica*, **1**, 391–393.

Tinivella, U. & Accaino, F. 2000. Compressional velocity structure and Poisson's ratio in marine sediments with gas hydrate and free gas by inversion of reflected and refracted seismic data (South Shetland Islands, Antarctica). *Marine Geology*, **164**, 13–27.

Tinivella, U. & Carcione, J.M. 2001. Estimation of gas-hydrate concentration and free-gas saturation from log and seismic data. *The Leading Edge*, **20**, 200–203.

Tinivella, U., Accaino, F. & Lodolo, E. 1998a. Reflected and refracted seismic images of the BSR in the South Shetland Margin (Antarctic Peninsula). *Annales Geophysicae*, **16** (Suppl. 1), C299.

Tinivella, U., Lodolo, E., Camerlenghi, A. & Boehm, G. 1998b. Seismic tomography study of a bottom simulating reflector off the South Shetland Margin (Antarctica). *In* Henriet, J.-P. & Mienert, J., *eds*. *Gas hydrates: relevance to world margin stability and climate change*. *Special Publication of the Geological Society of London*, No. 137, 141–151.

Tucholke, B.E., Bryan, G.M. & Ewing, J.I. 1977. Gas hydrate horizons detected in seismic-profile data from the Western North Atlantic. *American Association of Petroleum Geologists Bulletin*, **61**, 698–707.

Whalley, E. 1980. Speed of longitudinal sound in clathrate hydrates. *Journal of Geophysical Research*, **85**, 2539–2542.

Appendix A

Biot-Gassmann Theory (BGT)

Elastic velocities (i.e. compressional-velocity (V_p) and shear velocity (V_s)) of water-saturated sediments can be computed from the elastic moduli by the following formulas:

$$V_p = \sqrt{\frac{k + 4\mu/3}{\rho}} \quad \text{and} \quad V_s = \sqrt{\frac{\mu}{\rho}} \qquad (1)$$

where k, μ, and ρ are bulk modulus, shear modulus, and density of the formation, respectively. The formation density is given by

$$\rho = (1 - \phi)\,\rho_{ma} + \phi\,\rho_{fl,} \qquad (2)$$

https://doi.org/10.1017/S0954102003001275 Published online by Cambridge University Press

where ϕ, ρ_{ma} and ρ_{fl} are the porosity, matrix density , and pore fluid density, respectively.

The bulk and shear moduli are given by the following formuli using the Biot coefficient ß (Lee, unpublished data)

$$k = k_{ma}\,(1-\beta) + \beta^2 M.$$

$$\mu = \frac{\mu_{ma} k_{ma}(1-\beta)(1-\phi)^2 + \mu_{ma}\beta^2 M(1-\phi)^2}{k_{ma} + 4\mu_{ma}\left[1-(1-\phi)^2\right]/3}. \quad (3)$$

where

$$\frac{1}{M} = \frac{(\beta-\phi)}{k_{ma}} + \frac{\phi}{k_{fl}}, \quad (4)$$

and k_{ma}, μ_{ma}, and k_{fl} are the bulk modulus of matrix, the shear modulus of the matrix, and the bulk modulus of the fluid respectively.

For soft formations or unconsolidated sediments, the following Biot coefficient was used (Lee 2002)

$$\beta = \frac{-184.05}{1+e^{(\phi+0.56468)/0.10817}} + 0.99494 \quad (5)$$

For hard formations or consolidated sediments, the equation by Raymer *et al.* (1980), which is written by the following form by Krief et al. (1990), was used.

$$\beta = 1-(1-\phi)^{3.8} \quad (6)$$

Velocities of non-gas-hydrate-bearing sediments can be calculated using above equations. The effect of the gas hydrate on the elastic velocities is modelled such that gas hydrate acts as part of the frame or the skeleton (Helgerud *et al.* 1999). The elastic moduli of the composite matrix are computed by the Hill's average equation (Hill 1952).

https://doi.org/10.1017/S0954102003001275 Published online by Cambridge University Press